The BMRC/NCAR C-Band Polarimetric (C-POL) Radar System

T. KEENAN, K. GLASSON, AND F. CUMMINGS

Bureau of Meteorology Research Centre, Melbourne, Victoria, Australia

T. S. BIRD

Commonwealth Scientific and Industrial Research Organisation, Telecommunications and Industrial Physics, Epping, New South Wales, Australia

J. KEELER AND J. LUTZ

National Center for Atmospheric Research, Boulder, Colorado

(Manuscript received 27 February 1997, in final form 3 October 1997)

ABSTRACT

The development of the first Australian C-band polarimetric/Doppler meteorological radar system (C-POL) is described. Motivated by the need to obtain improved rainfall estimation and the vertical profile of hydrometeors, C-POL was developed jointly by the Bureau of Meteorology (BOM), the Commonwealth Scientific and Industrial Research Organisation of Australia, and the National Center for Atmospheric Research. C-POL is based on a standard operational C-band radar employed by the BOM but modified to be capable of transmitting linear horizontal and vertical polarizations and receiving the co- and cross polarizations on a pulse-to-pulse basis. Standard variables extracted include horizontal reflectivity (Z_{HH}), radial velocity (V_r), spectral width (σ_v), differential reflectivity (Z_{DR}), differential phase shift (Φ_{DP}), and zero lag correlation coefficient [$\rho_{HV}(0)$]. With the addition of a second receiver chain, the linear depolarization ratio will soon be available.

Initial results with the radar are discussed to give examples of the data quality, as well as some of the problems inherent in using a C-band radar in the Tropics.

1. Introduction

An observing station has been established near Darwin, Australia (11°S, 131°E), as part of the Tropical Rainfall Measuring Mission (TRMM) (Simpson et al. 1988) to provide information on tropical rainfall. This area has a monsoon climate affected by oceanic and continental convective systems and has been employed in a number of studies, providing quantitative measurements of rainfall for the TRMM ground validation program.

The characteristics of radiation sensed by satellites are in part determined by the vertical distribution of hydrometeors. At present, systematic study of the vertical distribution of hydrometeors in tropical precipitation systems is limited. As discussed by Jameson and Johnson (1990), polarized radars can infer many microphysical properties of precipitating clouds, such as particle size, shape, and phase. Polarimetric radars also offer significant advantages for rainfall estimation as discussed by Doviak and Zrnić (1993). This attribute is also important for TRMM ground validation studies.

Hence as part of the Bureau of Meteorology Research Centre (BMRC) TRMM ground validation program, a C-band dual-polarized radar system has been developed. The strategic aims of this development were to further our understanding of the vertical distribution of hydrometeors[1] within tropical convective systems and to undertake research relevant to radar-based rainfall measurement. The design and evolution of this polarimetric radar system and some initial results that characterize its performance will be described in this paper. First data were obtained during the recent Maritime Continent Thunderstorm Experiment (MCTEX) described by Keenan et. al. (1994).

2. System design and characteristics

In support of the BMRC research activities in Darwin the first Australian Doppler weather radar system was

Corresponding author address: Dr. Thomas D. Keenan, Bureau of Meteorology Research Centre, GPO Box 1289K, Melbourne, Victoria 3001 Australia.
E-mail: t.keenan@bom.gov.au

[1] Radar-detected hydrometeors in this case.

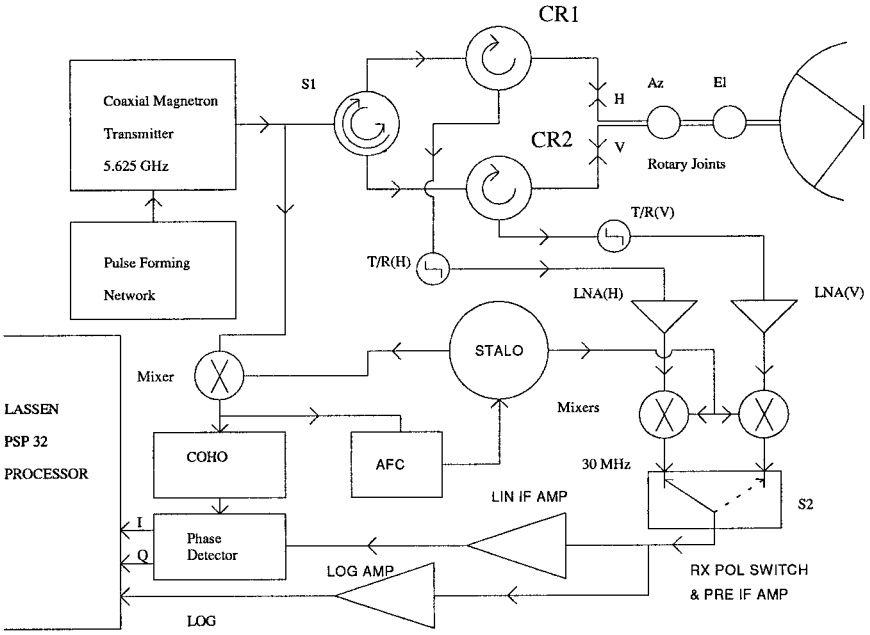

FIG. 1. Schematic of the C-POL radar system. The transmitted polarization is achieved through use of the ferrite switch S1. Circulators CR1 and CR2 switch energy through either the transmit or receive channels. Switch S2 selects the polarization mode processed by the receiver.

TABLE 1. C-POL system characteristics.

Antenna	
Size	4.2-m center-fed paraboloid
Beamwidth	1.0°
Gain	45 dB
Max sidelobe	<25 dB
Max cross polar	<−30 dB
ICPR	<−35 dB
Transmitter	
Pulse magnetron	250 kW peak
Pulse width	1.0–2.0 μs
Pulse rates	200–1200 Hz
Frequency	5625 MHz
Receiver	
Balanced coaxial receiver	
Single channel (co- or cross polar)	
Minimum detectable signal <−115 dBm	
Minimum detectable reflectivity* at 10 km −29 dBZ	
Bandwidth 0.5/1.0 MHz	
Channel isolation > 30 dB	
Polarizations	
Linear, horizontal and vertical	
Pulse-to-pulse control	
Ferrite switch on transmit	
Variables: Z_{HH}, V_r, σ_v, Z_{DR}, Φ_{DP}, $\rho_{HV}(0)$, LDR	
Computer	
Sun Sparc 96-MB memory	
5-Gb Disk	
Exabyte tape archive	
Display	
40-cm color monitor	
Mouse control	

* Assuming no path attenuation, etc.

developed by the Bureau of Meteorology (BOM) by modification of a standard 1° beamwidth C-band Enterprise Electronics Cooperation (EEC) radar system. The transmitter, which is fitted with a coaxial magnetron and stabilized high voltage power supply was modified by the addition of the necessary coherent oscillator (COHO). The receiver employed an in-house-developed low noise receiver with a minimum detectable signal of −115 dBm. A Lassen data acquisition, display, and archive system was acquired and modified to function with this radar. This resulted in a fully functional and integrated research quality Doppler radar. This Doppler radar had been operating in Darwin since 1993, providing ground validation data for the TRMM program.

Given cost restrictions, a polarimetric capability based on an upgrade to the existing Doppler radar had to be considered. This was advantageous in that technical support for the system would be available assuming a basic compatibility with radars maintained by BOM.

The choice of polarization method basically revolved around use of circular, linear, or say ''slant,'' etc., modes. The relative advantages are discussed by Holt (1995). For the C-band polarimetric/Doppler meteorological radar system (C-POL), a linear polarization approach seemed appropriate given the existing system. The variables deemed important included the horizontal (Z_{HH}) and vertical radar reflectivities (Z_{VV}) defined as

$$Z_{HH} = \frac{\lambda^5}{\pi^5 |k|^2} \int \sigma_{HH} N(D)\, dD \quad (\text{mm}^6\ \text{m}^{-3}) \quad \text{and} \quad (1)$$

$$Z_{VV} = \frac{\lambda^4}{\pi^5 |k|^2} \int \sigma_{VV}(D) N(D)\, dD \quad (\text{mm}^6\ \text{m}^{-3}), \quad (2)$$

where σ_{HH}, σ_{VV} are the radar cross sections at horizontal (H) and vertical (V) copolar states, $N(D)$ is the particle size distribution, λ is the radar wavelength, and $k = (\epsilon - 1)/(\epsilon + 1) - 1$, where ϵ is the complex relative permittivity of the particle. The differential reflectivity Z_{DR} is defined as

$$Z_{DR} = 10 \log \frac{Z_{HH}}{Z_{VV}}. \quad (3)$$

The linear depolarization ratio (LDR) is defined as the ratio of the cross-polar signal power to the copolar power:

$$\text{LDR} = 10 \log \frac{Z_{HV}}{Z_{VV}}. \quad (4)$$

The zero lag cross-correlation coefficient $[\rho_{HV}(0)]$, which is for backscatter amplitudes S_{HH} and S_{VV}, is related to the cross-correlation coefficient ρ_{HV} as follows:

$$\rho_{HV} = \frac{\int S^*_{HH}(D) S_{VV} N(D)\, dD}{\left[\int |S_{HH}|^2 N(D)\, dD\right]^{0.5} \left[\int |S_{VV}|^2 N(D)\, dD\right]^{0.5}}, \quad (5)$$

where $\rho_{HV} = \rho_{HV}(0) e^{i\delta}$, $\rho_{HV}(0)$ is the magnitude of ρ_{HV} and δ is the backscatter differential phase shift. The specific differential phase K_{DP} for forward scatter amplitudes f_{HH} and f_{VV} is defined as follows:

$$K_{DP} = \frac{2\pi}{k_0} \text{Re} \int [f_{HH} - f_{VV}] N(D)\, dD \quad (\text{deg km}^{-1}), \quad (6)$$

where k_0 is the free-space propagation constant and the two-way differential propagation phase shift (Φ_{DP}) between ranges r_1 and r_2 is defined as

$$\Phi_{DP} = 2 \int_{r_1}^{r_2} K_{DP}(r)\, dr \quad (\text{deg}). \quad (7)$$

Other variables required included the radial velocity (V_r) and spectrum width (σ_v).

The operation at C band meant that a large, costly, and bulky system—for example, as associated with S-band systems—was not an inevitable consequence. Propagation effects are also larger at C band than at S band. This is advantageous in the sense that it reduces the minimum detectable rain rate (since phase shift is inversely related to wavelength) that can be inferred from Φ_{DP}. The corollary is greater susceptibility to unwanted propagation effects, such as attenuation and Mie scattering. However, as shown by Aydin and Giridhar (1992) and demonstrated later, these deleterious effects (at least attenuation and differential attenuation) can be mitigated partially by use of Φ_{DP}. Hence, design options based on upgrading the existing Doppler radar facility to provide co- and cross-polar measurements using linear horizontal and vertical polarization states were considered.

FIG. 2. Photograph of C-POL as deployed during MCTEX 1995.

Issues relevant to the development of a meteorological polarimetric radar are discussed in detail by Ussailas and Metcalf (1983). The antenna typically represents a primary limitation to overall performance. For instance, measurement of LDR requires a low value (< -30 dB) of the integrated cross-polar ratio (ICPR).[2] However, low copolar sidelobe performance is also critical. Herzegh and Carbone (1984) show problems that develop from this source for Z_{DR} measurements in regions with large reflectivity gradients. Sachidananda and Zrnić (1987) also pointed out that the phase of the signal is more susceptible to contamination from sidelobes.

Ussailas and Metcalf (1983), Chandrasekar and Keeler (1993), and Xiao et el. (1993) summarize antenna design requirements, while characteristics of antenna systems employed in functional polarimetric radars are given by Bringi and Hendry (1990). It is impossible to achieve an antenna with no sidelobes, infinite cross-polar isolation, and identically matched illumination patterns.

A good technical approach for low sidelobes is to use an offset reflector. This eliminates a feed blockage problem inherent in front-fed paraboloids (a source of deleterious diffraction decreasing overall main lobe purity and cross-polar isolation) as well as providing less off-axis energy to the reflector and thus maximizing the cross-polar isolation. However, even at C band, where a 1° beamwidth scanning radar is required, such systems can be expensive, extremely large, and involve heavy supporting and robust drive mechanisms. The result is a radar susceptible to antenna wind loading with limited portability. The former limits pointing accuracy and the range of environmental conditions under which the radar

[2] Defined as the ratio of the integrated cross-polar energy to copolar energy emitted by antenna.

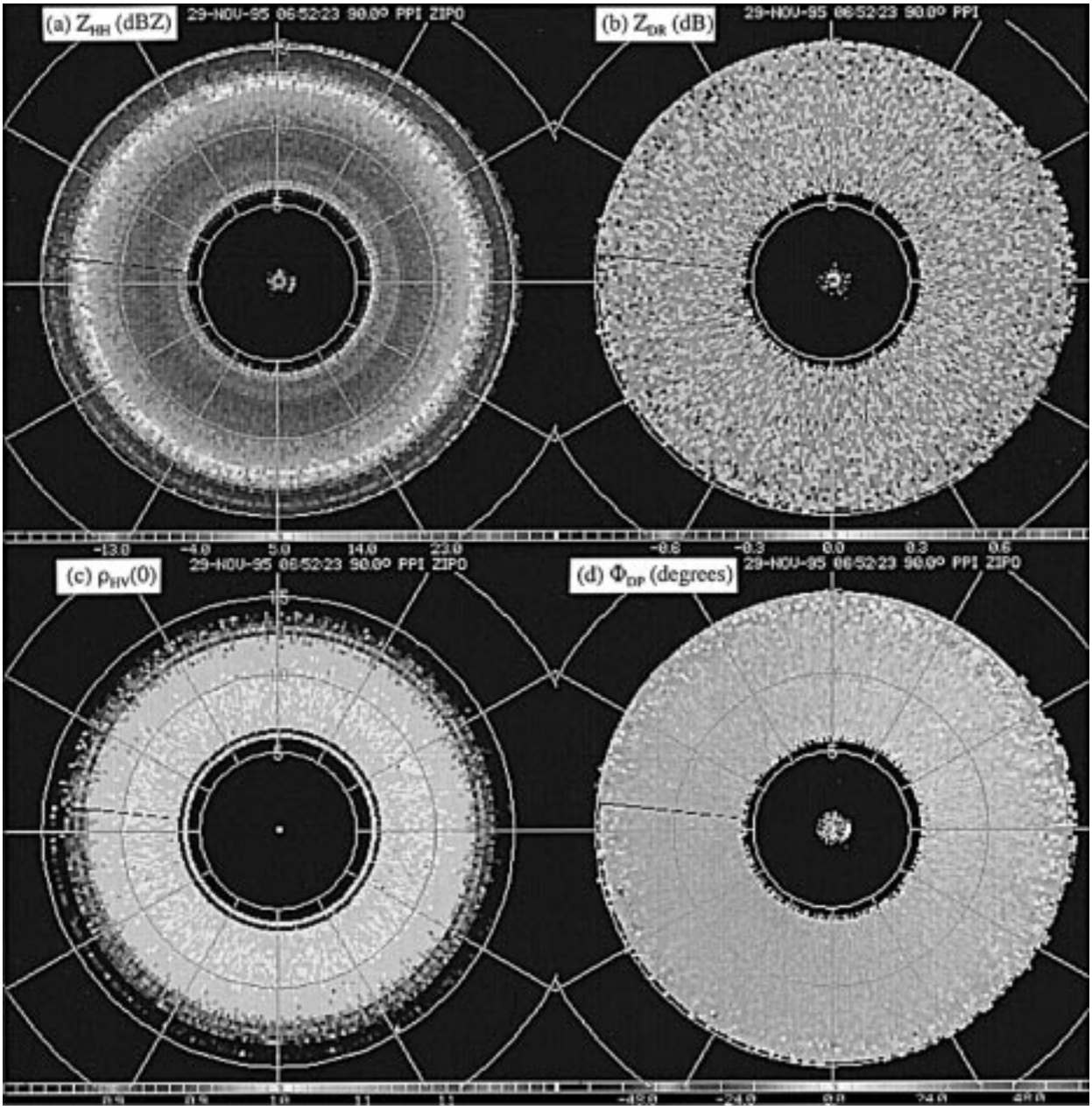

FIG. 3. Vertically pointing 360° scan data collected through the trailing stratiform of a thunderstorm on 29 November 1995: (a) Z_{HH} (dBZ), (b) Z_{DR} (dB), (c) $\rho_{HV}(0)$, and (d) Φ_{DP} (degrees). Tables for each variable are given. Range rings every 5 km.

can operate (assuming operation is without a radome, which is also desirable). These reasons together with cost and the basic incompatibility of such systems with the BOM network radars led to this approach not being adopted.

In practice an effective antenna that has reasonably matched amplitude and phase characteristics for the main lobe with low sidelobes for each polarization and a low ICPR can be obtained with a center-fed parabolic dish. Although not ideal, this less expensive and technically simpler approach overcomes many of the practical problems inherent with an offset-fed antenna. Values achievable with a carefully constructed center-fed antenna are summarized in detail by Mueller et al. (1995), where first sidelobe levels of -27 dB were achieved with a well-matched lobe structure. This is extremely important for accurate and artifact-free measurement of Z_{DR}, as discussed by Herzegh and Carbone (1984). Low ICPR (<-32 dB) is also necessary for quality depolarization measurements. These goals were deemed achievable for C-POL.

System cross-polarization isolation must be at least

as large as that obtained by the actual cross-polar signals from the meteorological echoes. Typically, the antenna represents the limit in this sense, although careful design is necessary to avoid coupling between channels in the polarization switch, cables, and other system components in the transmitter and receiver chain. The performance of a ferrite polarization switch is usually the limiting factor and this is dependent on many things, including its location, temperature, system duty cycle, etc.

The basic C-POL design is illustrated in Fig. 1 and technical characteristics are summarized in Table 1. The system employs a latching circulator (Raytheon ferrite switch denoted by S1 in Fig. 1) to alternate on a pulse-to-pulse basis the polarization mode of the transmitted energy. A dual-waveguide run feeds a center-fed paraboloid dish with a diameter of approximately 4.2 m. Linear horizontal and vertical polarization modes are available with this approach. Dual-channel rotary joints are employed on both waveguide runs through the pedestal to the antenna and feed. In the receive mode, circulators CR1 and CR2 simultaneously switch horizontal and vertical polarized received energy through separate channels employing low noise amplifiers [see LNA(H) and LNA(V) in Fig. 1]. The receiver chain is protected during transmission by the transmit/receive cells (T/R). The low power switch (S2) is used to select the polarization mode directed to the receiver and processor chain. At present only a single receiver chain is employed. The advantages of this basic design include the following.

1) The crucial latching circulator S1 is located in a controlled atmosphere (within the air-conditioned environment of the radar transceiver) and not exposed to the elements as it would be with an antenna-mounted circulator. This provides a protected and stable temperature environment for the latching circulator and, as a result, optimal isolation is maintained and insertion losses are minimized.
2) The system is potentially configured for dual-receiver operation, enabling simultaneous processing of co- and cross-polar signals.
3) The fast-latching circulator is employed only for isolation on the transmit cycle, which enables isolation optimization. Cross-polar isolation is approximately 35 dB, which is comparable with the best results achievable with present antenna systems. Hence the latching circulator is not necessarily the ultimate limit to the cross-polar isolation achievable within the system.

C-POL operation can be configured to operate in either traditional Doppler mode, where the whole dual-polarization switching configuration is bypassed (not shown in Fig. 1) or in a complete dual-polarization/Doppler mode. The mode selection is achieved by computer control under the scan scheduler. The bypass mode is available to optimize overall system sensitivity by bypassing the ferrite circulator and feeding the transmitter pulse directly to the horizontal antenna feed port.

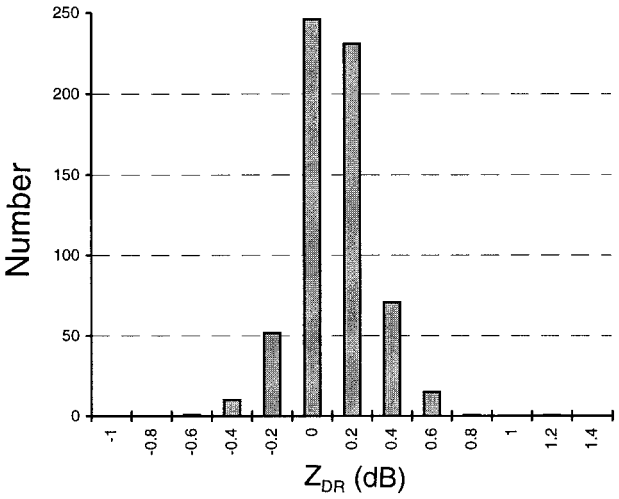

FIG. 4. Histograms of Z_{DR} for the data presented in Fig. 3.

A UNIX-based Lassen Research radar processor (Sun Force board on VME bus) with a fully programmable PSP 32 signal processor, radar control, data acquisition (RADEX), and display system (SUNrise) form the basic hardware/processing configuration. Up to 1000 range gates can be accommodated within the Lassen PSP 32 signal processor with a pulse width up to 2 μs and a typical pulse repetition time (PRT) of 1 ms. Range sample gates for the system vary from 75 to 1800 m in spacing, but for the majority of data are set at 300 m.

All receiver and Lassen system changes necessary to obtain research quality functionality were undertaken in-house. The receiver was designed and constructed with a polarization selectable dual front end to produce the logarithmic and the in-phase (I) and quadrature (Q) video signals. Two new low noise figure (NF) and moderate gain LNAs were added to the receiver. COHO was designed to lock in at less than 1 μs, to have a quick start, and to exhibit high Q characteristics for low phase noise operation. The intermediate frequency (IF) preamplifier was given a moderate gain in order to restrict the power driven through the following stages but high enough to maintain the system NF with the initial gain control turned off. The linear IF amplifier was given just enough gain to drive the I and Q demodulator and to minimize the NF degradation and phase change over its dynamic range. Gain compression was used to match the difference in dynamic range between the C-POL system and the Lassen processor. An in-house-developed low noise wide dynamic range I and Q demodulator was designed with matched linear phase filters incorporating good image rejection ($>$30 dB). The logarithmic amplifier was constructed with 80 dB of dynamic range with an accurate conversion look-up table and matched band-limiting filters. The receiver NF was 1.7 dB with 90 dB of dynamic range with 60 dB being

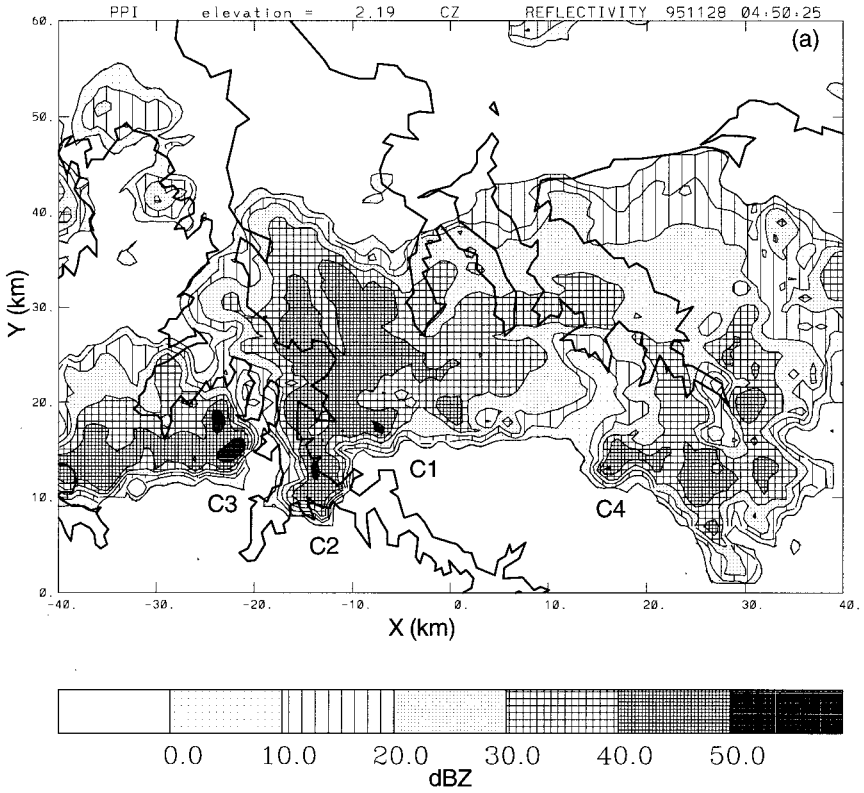

FIG. 5. C-POL observations at 0450 UTC 28 November 1995 during MCTEX: (a) Z_{HH} (dB), (b) Z_{DR} (dB), and (c) Φ_{DP} (degrees). Radar tilt angle is 2.2° and coastal outline of Tiwi Islands is indicated.

managed in a window by sensitivity time control over the first 100 km.

The IF system and COHO were tested initially using signal generators to simulate the radar data and a segmented memory digital storage oscilloscope to view the **I** and **Q** vectors. These vectors were plotted at a pulse repetition frequency (PRF) of 300 Hz for 200 samples at a range of 200 km. Peak-to-peak phase noise was less than approximately 10°. Subsequent analysis of the data (see section 5 and Fig. 6b) indicated the complete system rms phase noise was approximately 3.8°.

Development of the polarization switching system and an initial antenna upgrade were undertaken in collaboration with the Commonwealth Scientific and Industrial Research Organisation (CSIRO). The existing EEC antenna was modified for dual polarization by replacing the feed system and rotary joints. A new ring-slot feed and circular orthogonal mode transducer were developed for low cross polarization and high return loss. The rotary joints used a concentric coaxial design that maximized the peak power capability in both channels. Detailed radiation measurements were made at CSIRO using a Fresnel-zone technique, and these gave two-dimensional far-field patterns and reflector surface data. These data showed that while the upgraded antenna had low cross polarization (peak < -32 dB, ICPR < -34 dB), larger than expected copolar sidelobes (~ -21 dB below the peak) were obtained in the vertical plane. Analysis indicated that reflector distortions (1.6-mm rms and ± 3-mm peak) and blockage due to the feed waveguide run caused the problem. To overcome these antenna limitations, a pedestal and Ericsson antenna with dual-polarization feed owned by the National Center for Atmospheric Research (NCAR) were lent to BMRC for use on C-POL in an attempt to overcome these antenna limitations. With the NCAR pedestal, use of a radome was not required and this was an additional benefit because radomes tend increase the sidelobe level, reduce gain (especially when wet), and cause depolarization (Cary 1986).

A research-quality radar that could operate in a variety of field projects was necessary, so for flexibility the system was designed to be as highly portable as possible. Two 20-ft sea containers located side by side are employed for mounting the pedestal. At present all the radar equipment is housed in one air-conditioned sea container. The other is employed for storage, etc. A third smaller container houses a diesel generator. This generator can power the whole system. C-POL can be operated on external power or exclusively from the generator. An uninterruptable power supply has also been installed and will invoke automatic use of the generator

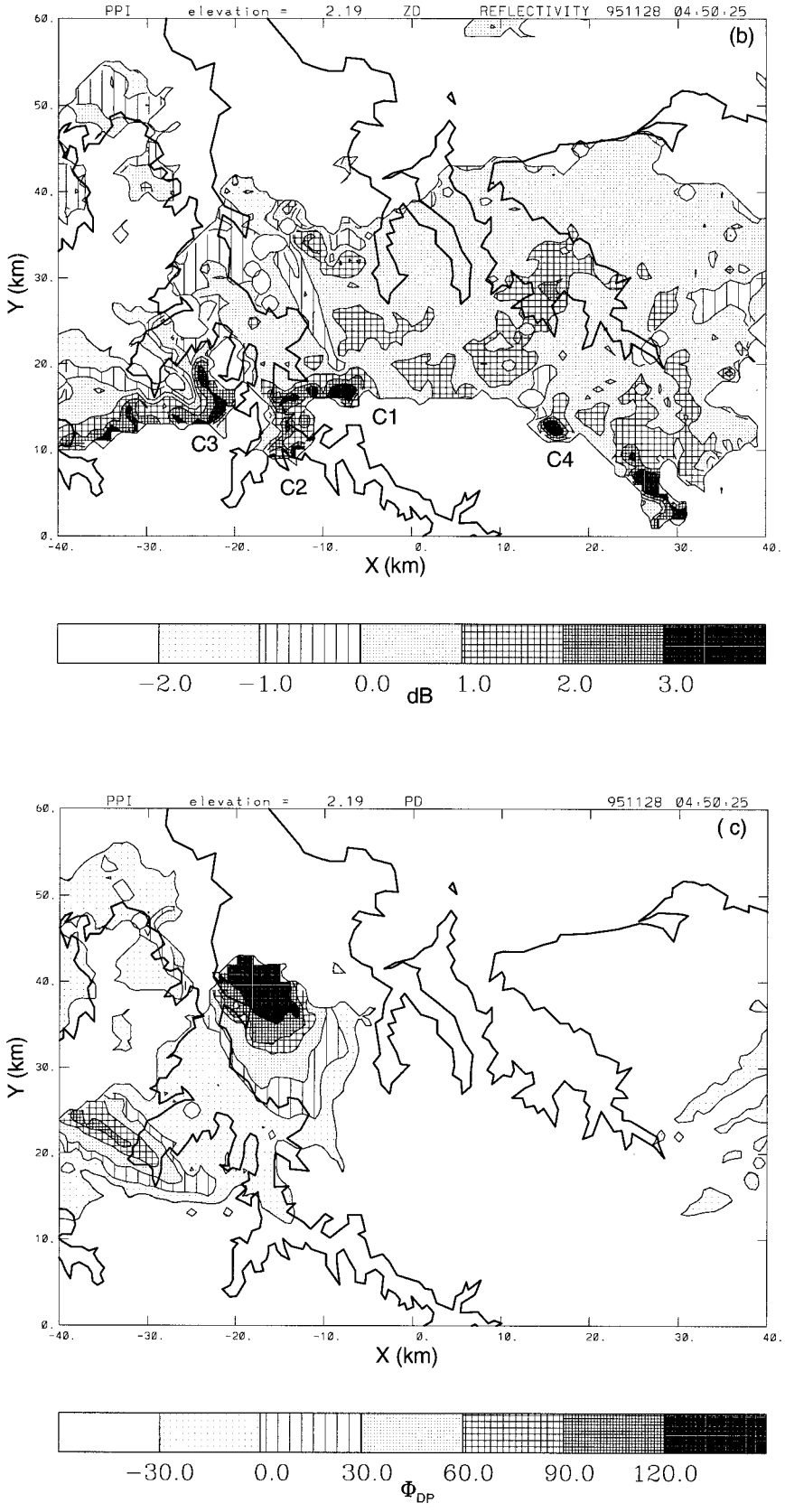

FIG. 5. (*Continued*)

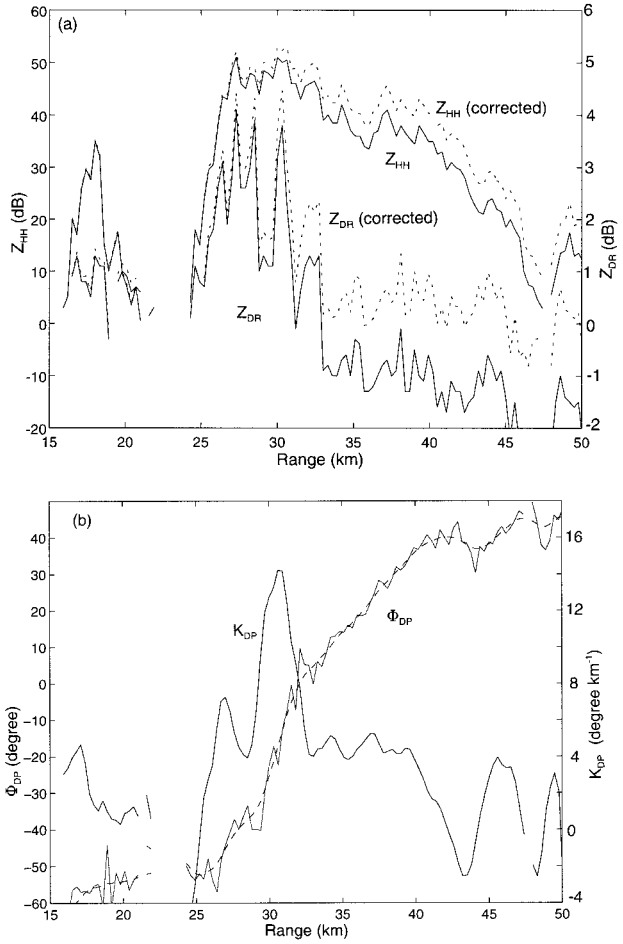

FIG. 6. C-POL radial data through cells C2 and C3 (Fig. 5): (a) Z_{HH} and Z_{DR} before (solid) and after (dashed) Φ_{DP} attenuation correction. (b) Raw and smoothed Φ_{DP}. Here, K_{DP} is also indicated.

in the case of an external power failure. The system was deployed at a remote location near Darwin, Australia, during the 1995 MCTEX (Keenan et al. 1994) and is shown in Fig. 2.

It is relevant to consider where C-POL stands in relation to other polarimetric radar facilities. Technical aspects and capabilities of a wide range of polarimetric radars are summarized in detail by Bringi and Hendry (1990) and Collier (1995). Systems have been developed for operating frequencies between 3 and 35 GHz with a variety of polarization states. In the United States most are S-band radars. Of relevance to C-POL are a number of European C-band systems, including the Deutsche Forschungsanstalt für Luftund Raumfahrt (DLR) polarimetric radar, which has the capability to measure the full scattering matrix.

Prior to 1990, real-time measurement of polarimetric variables requiring estimates of returned power and Doppler frequency shift meant separate radar scans to recover the respective variables. This limited the operating flexibility of these early radars. Time series data were often employed for the extraction of Doppler-related variables, again placing restrictions to the amount of data collected. With ongoing improvements in computer technology and the algorithm described by Zahrai and Zrnić (1993), it became easy to employ linear H and V polarization states to extract in real time Doppler-based and power-based polarimetric variables simultaneously. Upgrades in the capabilities of existing radars inevitably resulted. At S band, Zahrai and Zrnić (1993) presented results with this new technique employing the Cimmaron radar. The development described herein is the first to employ this capability at C band.

Additional configuration changes have also developed. For instance the S-band Colorado State Iniversity, University of Chicago, and University of Illinois facil-

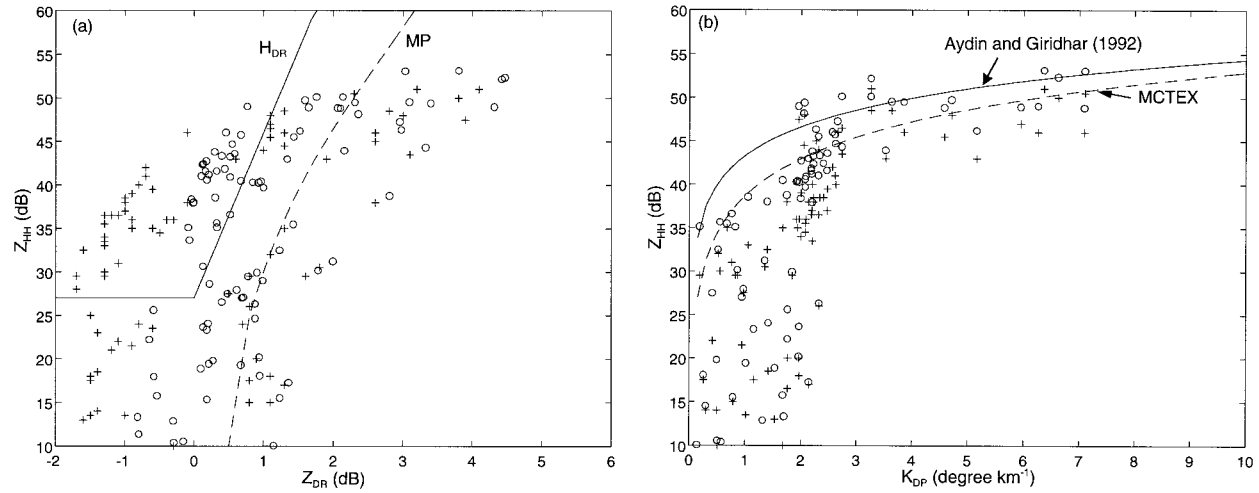

FIG. 7. Scatterplots of C-POL data along the radial through C2 and C3 (see Fig. 5) before (crosses) and after attenuation correction (circles). (a) Z_{HH} (Z_{DR}): solid line is the differential hail signal (H_{DR}) of Aydin and Giridahar (1992) and dashed curve is relation from Marshall–Palmer (1948) drop size distribution. (b) Z_{HH} (K_{DP}): solid line is Aydin and Giridhar (1992) curve and dashed line (MCTEX) is best fit to present data.

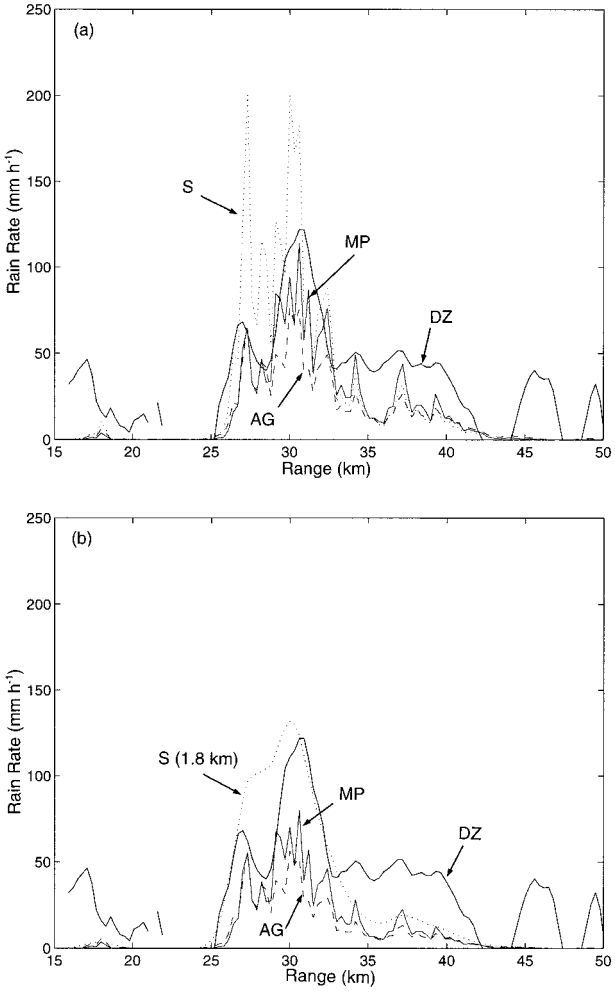

FIG. 8. Comparison of radar rainfall estimates along ray through C2 and C3 (see Fig. 5). For $R(Z_{HH}) = 0.0167Z_{HH}^{0.800}$ (S) following Steiner et al. (1995); $R(Z_{HH}) = 0.0365Z_{HH}^{0.625}$ (MP), following Marshall–Palmer (1948); $R(Z_{HH}, Z_{DR}) = 0.00237Z_{HH}^{0.95}Z_{DR}^{-1.17}$ (AG) following Aydin and Giridhar (1992); and $R\ (K_{DP}) = 22.32K_{DP}^{0.866}$ (DZ) following Doviak and Zrnić (1993). (a) With polarimetric attenuation correction applied to reflectivity measurements and (b) without polarimetric attenuation correction and 1.8-km smoothing applied to S estimates.

ity, described by Mueller et al. (1995), now employs dual transmitter and receivers, alleviating the need for a ferrite switch. The portable S-POL system, described by Lutz et al. (1995), has also been developed without the need for a ferrite switch. As discussed, the isolation performance of the ferrite switch was important only for the transmitted energy and did not present a design limitation for C-POL. Additionally, all required polarimetric variables were available with the implementation of the second receiver option.

C-POL is therefore considered a unique C-band system building on technical advantages that have occurred over recent years. It is based on the use of linear H and V states with a dual-receiver design for simultaneous two-channel reception, although the single-channel version has been implemented only to this stage. It does not have the full polarimetric diversity capability of say the DLR system but represents a portable system capable of measuring the most frequently employed and understood polarimetric variables. It is also an example of a polarimetric system that evolved from a conventional noncoherent radar. Given the promise of polarimetric radar rainfall estimation techniques described by Zrnić (1996), there is likely to be more pressure for such adaptations in the future.

3. Signal processing and algorithms

The PSP 32 processor was modified to extract all the moments discussed previously. Radar reflectivity variables are recorded from the logarithmic IF receiver chain, with a receiver bandwidth of 1.35 MHz in short pulse mode (1 μs), and 0.64 MHz in long pulse (2 μs) mode. The PSP 32 processor converts the logarithmic video to a 12-bit digital sample through a front end analog-to-digital converter. This sample is then passed through a 4096 entry look-up table and converted to a floating point linear representation of received power (Chandrasekar et al. 1989). Integration over the selected number of sample pulses then occurs for improved accuracy. Postprocessing includes range normalization and conversion to dBZ for both unfiltered and clutter-filtered reflectivities.

For velocity data, the radar linear IF receiver chain is used to produce I and Q baseband converted signals using the 30-MHz COHO, phase locked to the transmitter pulse. The I and Q signals are fed to the PSP 32 input where they are converted to 12-bit digital data samples at each sample range.

In single polarization mode a standard linear pulse pair processing (PP) algorithm is applied to the I and Q data. For the spectrum width the standard PP variance estimator is employed. In dual-polarization mode, a modified PP algorithm is implemented to process the alternating H and V linear receiver I and Q signals following Zahrai and Zrnić (1993).

Here, Z_{DR} is computed as the difference (ratio) between horizontal and vertical logarithmic received powers. The ratio is then converted to decibels and corrections applied for other system calibration differences between the two channels.

The algorithm for Φ_{DP} extraction again followed Zahrai and Zrnić (1993), and Φ_{DP} is recorded in units of degrees, such that $-32° < \Phi_{DP} < +32°$ with folding occurring for angles outside these bounds—that is, $+33°$ is folded to $-31°$.

The algorithm for $\rho_{HV}(0)$ followed Zahrai and Zrnić (1993) except for the following variations. From Eq. (17) of Zahrai and Zrnić (1993), the calculation of $\rho_{HV}(T_S)^2$ not $\rho_{HV}(T_S)$ is performed as follows:

$$\hat{\rho}_{HV}(T_S)^2 = \left(\frac{|\hat{R}_a| + |\hat{R}_b|}{2\sqrt{\hat{S}_h \hat{S}_v}} \right)^2, \tag{8}$$

which is computed as

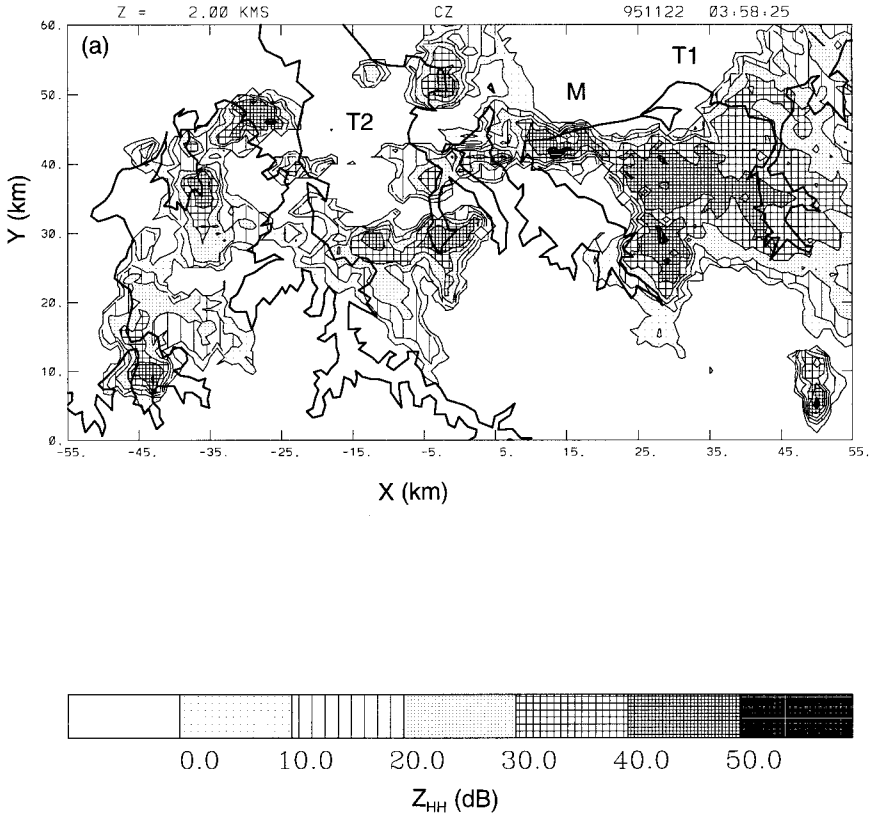

FIG. 9. C-POL data for 0358 UTC 22 November 1995 during MCTEX: (a) CAPPI of Z_{HH} (dB) at $z = 2.0$ km, (b) vertical cross section of Z_{HH} along $y = 40$ km in (a), (c) as per (b) but Z_{DR} (dB).

$$\hat{\rho}_{HV}(T_S)^2 = \frac{|\hat{R}_a|^2 + 2\sqrt{|\hat{R}_a|^2|\hat{R}_b|^2} + |\hat{R}_b|^2}{4\hat{S}_h\hat{S}_v}. \quad (9)$$

This was computationally much more efficient in the processor (one square root instead of three).

Then, to complete a modified Zahrai and Zrnić (1993) Eq. (18):

$$\hat{\rho}_{HV}(0)^2 = \frac{\hat{\rho}_{HV}(T_S)^2}{\sqrt{\hat{\rho}(2T_S)}}, \quad (10)$$

where $\rho(2T_s)$ is from Zahrai and Zrnić's Eq. (15), calculated using their Eq. (6). Here, $\rho_{HV}(0)$ is recorded in units of $\rho_{HV}(0)^2$ such that $0.3147 < \rho_{HV}(0)^2 < 1.3037$, which equates to $0.561 < \rho_{HV}(0) < 1.1418$.

The clutter correction for reflectivity data is applied by subtracting the clutter power estimated from the PP chain. The PP has provision for the application of a three-pole infinite impulse response digital filter with a user selectable filter width normally optimized for filter performance at the desired antenna rotation rate. The difference between the filtered and unfiltered linear powers is used to derive the clutter power correction applied to the logarithmic channel reflectivity powers. This filter has the effect of removing DC (zero velocity) components from the *I* and *Q* data within a user-selected spectral spread and typically results in approximately 27 dB of clutter suppression. The clutter filter has not been applied in dual-polarization mode at this stage.

All the radar variables and subsequent data products are stored separately in a single 8-bit character format for every range bin recorded. Data archival for the system is performed using a dual–high density Exabyte data storage system, which allows ''mirror'' archiving—that is, two copies of all data are recorded separately. Data are stored in a UNIX ''tar'' file format on the tapes and consist of volumes of radar data in a format designed by Lassen Incorporated.

4. Calibration

a. Power, velocity, and angle calibrations

Based on radar system calibration checks before and after MCTEX (specifically noise source and solar calibrations), the radar system gain factor showed a measurement variance of only 0.2 dB (i.e, 0.4-dB variation in the received power). These results indicated a very stable radar system and, considering the possible measurement variations and accuracy, suggested that adjustments to reflectivity data on system gain grounds were not warranted.

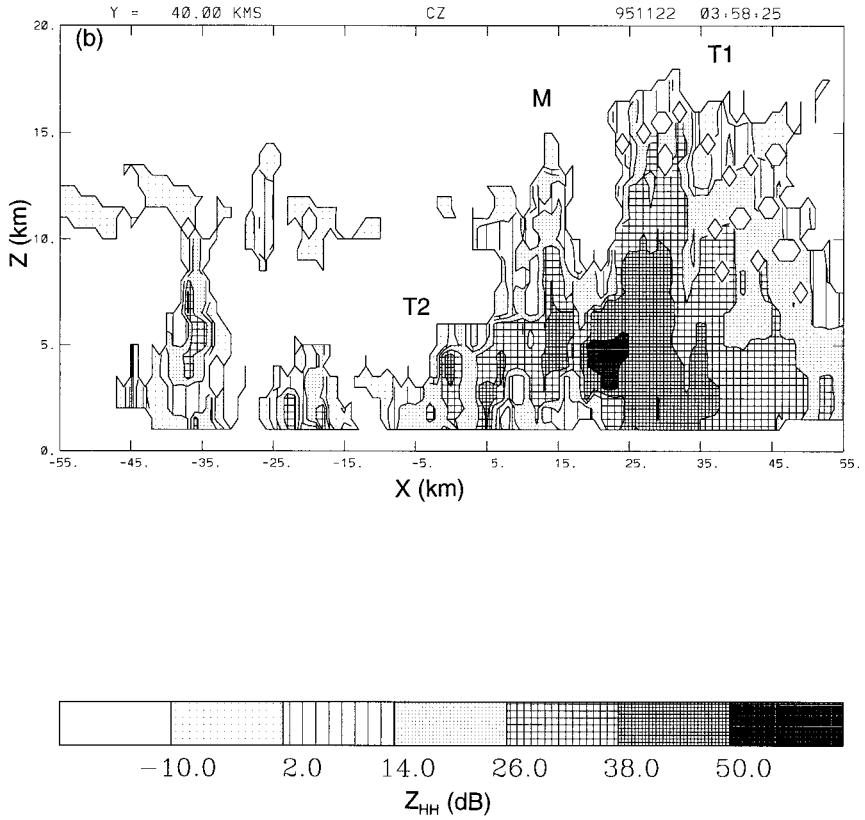

FIG. 9. (*Continued*)

The radar reflectivity calibration (Zcal) comparisons indicated the transmitter output power was quite stable with a maximum recorded variation of 0.2 dBm and typically approximately 0.1 dBm. This stability was due to a regulated high voltage power supply on the transmitter system. The radar receiver calibration performance was similarly quite stable with a maximum measurement difference of 0.25 dBm (0.3 dBm) in a dual-polarization (bypass/single polarization) mode. The variation was mainly at the extremities of the system operating range, and over most of the dynamic range of the receiver the variation was only 0.1 dBm.

There appear to be no obvious calibration problems with the velocity data. Coherent oscillator locking for permanent echoes consistently indicated zero rotation and minimal jitter as expected. Close agreement between velocity azimuth display-derived wind profiles and sounding data also provided ongoing confidence in the radial velocity estimates.

A single three-wire synchro position transmitter is used on each of the antenna azimuth and elevation axes. The analog angle information from these position transmitters is fed through 14-bit synchro-to-digital converters, which set the angular resolution of the system at 0.022° per bit. This digital information is stored as the ''binary'' angle for azimuth and elevation attached to each ray of data processed and is stored by the PSP 32 processor. Although 0.022° is the resolution of the system, it is not the overall accuracy as discussed below.

The angular spacing (resolution) of the data integrated and processed by the PSP 32 processor is fixed at 1.0° for full 360° plan position indicator type scans. The rotational rate of the antenna, the PRT, and number of samples determines the angular resolution for all other scan types. The angle attached to each integrated ray of data is the angle at the time of the start of the integration period.

Following Frush (1984), azimuth and elevation angle alignment is performed using the sun position as a reference. The sun tracking and angle alignment program is part of the antenna control computer package attached to the radar antenna interface. Angles are checked for alignment at the time of the solar calibrations, which are typically undertaken twice per month. No serious discrepancies are usually found, and the angle alignment accuracy can be taken as being within ±0.1°.

b. Radar timing considerations

The BMRC/Lassen PSP 32 processor uses a digital signal processor to control most of the radar-operating parameters—that is, pulse width, polarization mode, PRF, range sample gate timing, number of samples or angle boundary integration period, and control of the

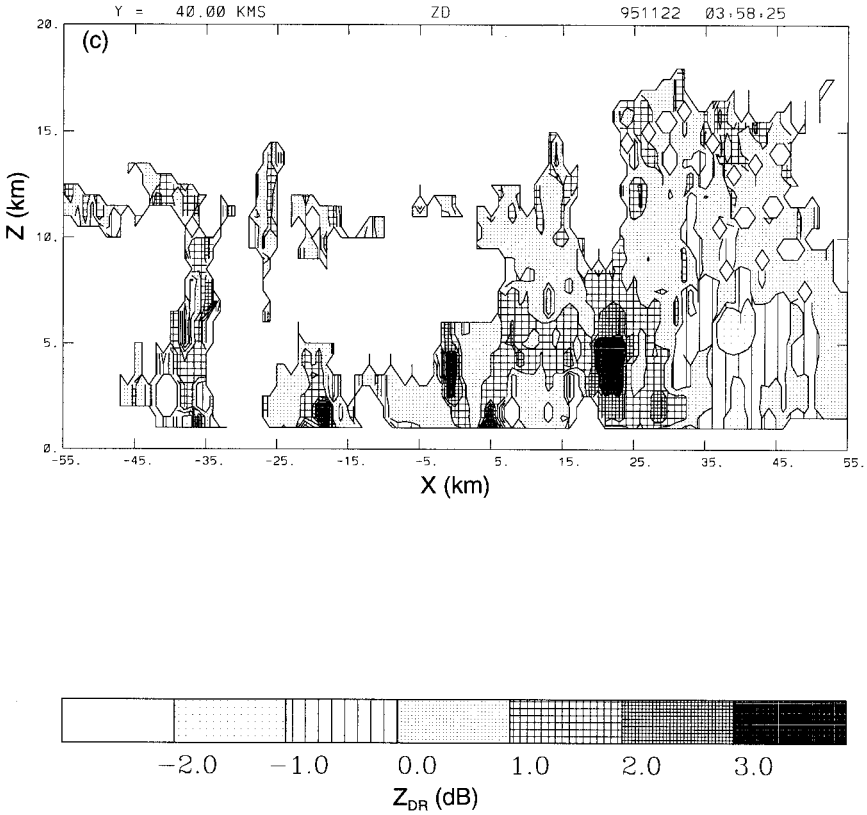

FIG. 9. (*Continued*)

gain control for the linear receiver chain. All of these functions are controlled by the sequencer program running in a dedicated DSP32C processor.

All of these parameters are checked periodically. Based on experience with the system and comparison with known ground targets, it is believed that at worst the range sampling should not be in error by more than a few tens of meters.

c. Meteorological calibration

As described by Zahrai and Zrnić (1993), useful inferences on the quality of the polarimetric data can be made by pointing the radar vertically and scanning the radar in azimuth during homogeneous rainfall to verify that no preferential alignment of hydrometeors exists. Under these conditions raindrops present spherical cross sections, which would result in $Z_{DP} = 0$ and constant Φ_{DP}. If such precipitation is unavailable, examination of ice in the anvil region of nonprecipitating cloud can be used as an alternative test.

The results from one such test employing a 360° of azimuth scan while pointing vertically is shown in Fig. 3. The raw data indicates extremely homogeneous fields from 6 to 12 km in height in the anvil region of a thunderstorm. The area-weighted mean value of Z_{DR} was 0.08 dB with 79% of values between ± 0.2 dB, as the histogram in Fig. 4 indicates. The Φ_{DP} values were also extremely constant without any obvious range dependency. Eighty-eight percent of the $\rho_{HV}(0)$ values are also greater than 0.97. These values are consistent with the meteorological expectation and imply good phase stability within C-POL.

5. First results

As mentioned, C-POL was deployed for the first time during MCTEX. The following data have been selected to demonstrate some characteristics of the first set of C-POL data.

a. Attenuation and rainfall

This example illustrates some of the problems inherent with a C-band polarimetric radar operating within the Tropics. In Fig. 5 a thunderstorm complex is evident extending some 40 km north of the radar (radar location in all diagrams is at the origin) with maximum Z_{HH} values of 40–50 dB*Z* in a line elongated almost north–south at $x = -15$ km. Cells C1, C2, C3, and C4 (Fig. 5a) have maximum reflectivities between 40 and 55 dB*Z* and maximum Z_{DR} (Fig. 5b) values in the range 3–5 dB*Z*. Through and behind these cores significant differential phase shifts are evident (see Fig. 5c), sugges-

tive of heavy rainfall with large drops. Behind cells C1, C3, and C4, wedge-shaped areas with decreasing and eventually negative Z_{DR} values are evident. This is indicative of significant differential attenuation.

The ray through cells C2 and C3 is presented in Fig. 6. Cell C3 at 30-km range has a peak Z_{HH} of 51 dB*Z*, an associated double peak Z_{DR} structure, and a $\rho_{HV}(0)$ minimum (not shown) of approximately 0.9. The maximum Z_{DR} values are approximately 4 dB*Z*! For a monodisperse drop size distribution, 5-mm diameter raindrops are necessary to produce such large Z_{DR} values. For a wavelength of 5 cm, this places the scattering within the Mie regime. The decreasing trend in Z_{HH} and Z_{DR} behind C3 again suggested significant attenuation of both the horizontally and vertically polarized signals (especially evident in the case of Z_{DR}, where negative values developed beyond the 32-km range). The two-way Φ_{DP} shown in Fig. 6b indicated an 85° phase shift through C3. The resulting K_{DP}[3] profile is consistent with the Z_{DR}-observed structure with a double peak associated with C3. Maximum K_{DP} values for C3 are 7.5° km^{-1} at 26 km, 12° km^{-1} at 31-km range, and approximately 4° km^{-1} behind C3. For C2, K_{DP} peaks at 5° km^{-1}. The negative K_{DP} values beyond 42.5-km range are associated with very low signals.

Relationships provided by Bringi et al. (1990) between Φ_{DP} and accumulated horizontal and differential attenuation can be used to correct for attenuation. The results of applying this procedure to Z_{HH} and Z_{DR} are shown in Fig. 6a. It is evident that substantial attenuation was occurring along this radial. Here Z_{HH} suffered up to 5 dB in attenuation and Z_{DR} at least 2 dB in differential attenuation. The attenuation correction also removed the negative Z_{DR} values observed in the raw data beyond the 32.5-km range. The peak K_{DP} value associated with C3 implied an attenuation rate of 0.7(0.2) dB km^{-1} for Z_{HH} (Z_{DR}). These results indicate there is potential for polarimetric techniques to overcome attenuation at C band.

A scatter diagram of Z_{DR} and Z_{HH} values along the ray through C2 and C3 is shown in Fig. 7a along with 1) the Aydin et al. (1986) hail signature (H_{DR}), and 2) a Z_{HH} (Z_{DR}) relationship employing a Marshall–Palmer (1948) distribution [assuming a maximum drop size of 8 mm and employing the Green (1975) raindrop oblateness relationship].

Before application of the attenuation correction procedure, the frequent occurrence of negative Z_{DR} values biased the sample in an unrealistic sense well to the left of the H_{DR} and MP curves. Values to the left of the H_{DR} curve imply the existence of hail. The fact that the radar beam is at heights(temperatures) between 0.5 (28°C) and 1.5 (20°C) km and the low frequency with which hail is reported at this tropical location makes it an unlikely scatterer. A significant amount of this bias was removed after the attenuation correction was applied with most of the Z_{HH}–Z_{DR} data (see Fig. 7b) within a regime consistent with rainfall and encompassing the general domain of the MP curve. However, many Z_{HH} and Z_{DR} pairs still fell to the left of the H_{DR} curve. A raindrop distribution dominated by large numbers of small drops, at least relative to the midlatitude case for which the H_{DR} curve was developed, could produce such an effect. The general applicability of the H_{DR} curve is therefore questionable. Additionally, attenuation not accounted for in the correction scheme could contribute to the effect. This is further explored in Fig. 7b where the observed reflectivities are plotted as a function of K_{DP}. The dashed line is a best fit to the data derived from a linear regression analysis of $\log(Z_{HH})$ and $\log(K_{DP})$ but only using corrected Z_{HH} values greater than 35 dB*Z*. The curve from Aydin et al. (1992) is also plotted. In general, the reflectivity values from the MCTEX data are 1–2 dB lower for a given K_{DP} than those of Aydin et al. (1992). Attenuation or less differential phase shift from a spectrum dominated by smaller drops could produce such an effect.

A comparison of radar-derived rain rates (R) for the radial through C3 is presented in Fig. 8. The following relationships were employed. Unless otherwise stated, the above attenuation correction procedure was first applied to all reflectivity estimates.

1) The Marshall–Palmer (MP) power law $Z_{HH} = 200R^{1.6}$.
2) The Steiner et al. (1995) (S) single power-law relationship ($Z_{HH} = 167R^{1.25}$) provided for the Darwin area. This is essentally a climatologically based gauge-corrected $Z_{HH}(R)$ relationship. No attenuation correction was applied.
3) The Aydin and Giridhar (1992) (AG) $R(Z_{HH}, Z_{DR})$ relationship ($R = 2.37 \times 10^{-3} Z_{HH}^{0.95} Z_{DR}^{-1.17}$).
4) The C-band R–K_{DP} relationship (DZ) $R = 22.32K_{DP}^{0.866}$, following Doviak and Zrnić (1993).

The overall trend from the four estimators was very similar, although there are substantial and significant differences between them. All reflectivity-based approaches were similar at rain rates less than 50 mm h^{-1} with the general order from highest to lowest being DZ, MP, S, and AG. The K_{DP} estimator was consistently 2–3 times larger than the reflectivity-based techniques in this ''low'' rain-rate regime. However, once the rain rate was greater than 50 mm h^{-1}, the S technique produced the highest rain rates followed by the K_{DP}-based DZ estimator. The K_{DP} estimator employed a range resolution of 1.8 km significantly less than the 0.3-km resolution of the reflectivity-based approaches. Once the S estimates are smoothed by a six-point running average to 1.8 km resolution, as shown in Fig. 8b, the peak rain

[3] To estimate the specific differential phase shift (K_{DP}) a six-point constant amplitude (1.8 km) zero phase shift forward and reverse filter was applied to the Φ_{DP} data with the results shown in Fig. 7b. Here, K_{DP} was then estimated from the derivative of this function with respect to range.

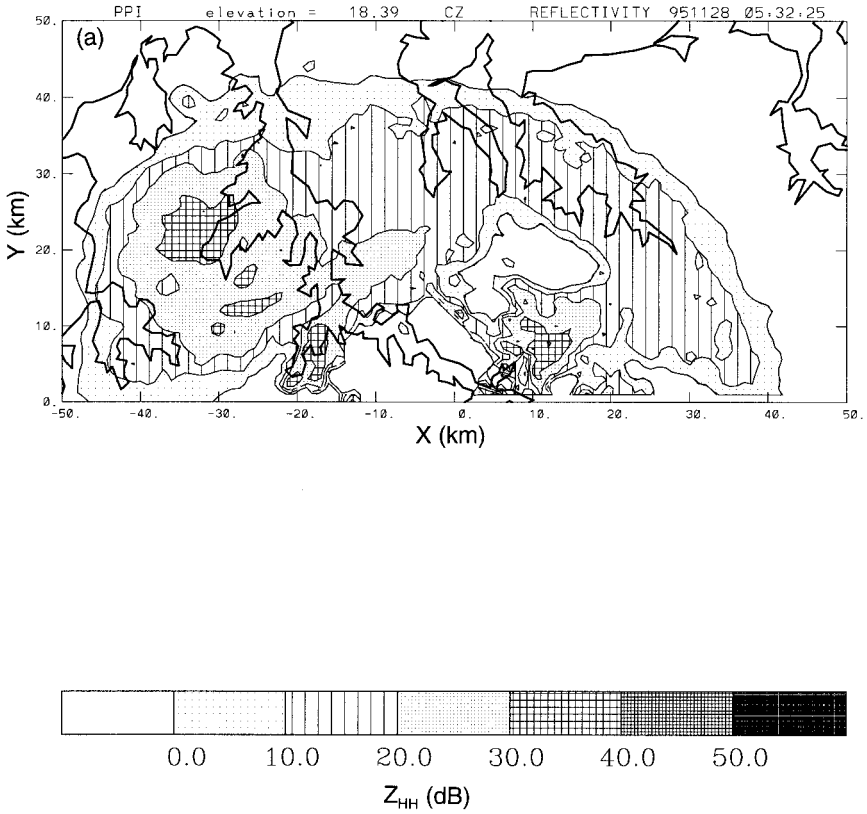

FIG. 10. C-POL data for 0532 UTC 28 November 1995 during MCTEX: (a) Z_{HH} (dB) at 18.4° elevation and (b) Φ_{DP} (deg) at 18.4° elevation. Arrows indicate location of decreasing Φ_{DP}.

rates from DZ and S are about the same. Further, as shown in Fig. 8b, without application of the attenuation correction, the MP and AG rain-rate estimates were at least half that of the K_{DP} and S estimates.

Here, K_{DP} is generally insensitive to drop size distribution variability, attenuation, and a number of other factors affecting the ability of radars to remotely sense rainfall. Results presented by Ryzhkov and Zrnić (1995) and Aydin et al. (1995) support these ideas and indicated that the K_{DP} rainfall estimator was quite robust, especially during high rainfall rates. The above has demonstrated that the rain rates from the K_{DP} and a gauge-corrected traditional reflectivity-based approach were internally consistent. In addition polarimetric attenuation correction procedures removed significant biases in traditional reflectivity-based approaches. Without the polarimetric capability, gauge corrections are necessary to obtain rain rates equivalent to the K_{DP}-based approaches. Work is now under way to validate these polarimetric rainfall estimates using rain gauges.

Further work is also under way exploring the relation between Φ_{DP} and differential attenuation and examining the impact of Mie scattering effects. Given the tropical location for C-POL with the frequent occurrence of large raindrops, the situation is likely worse than at higher latitudes.

b. Vertical storm structure

A vertical section of an island thunderstorm that occurred on 22 November 1995 during MCTEX is shown in Fig. 9. In this case a pre-existing thunderstorm complex (T1) was interacting with a sea-breeze front and developing new cells (M) aligned east–west ahead (along $y = 40$ for $5 < x < 25$) of the original complex. This was the start of a ''bridging'' process linking pre-existing cells to the west (T2 located west of $x = -5$) with the complex T1 located east of $x = 25$. One of the aims of MCTEX was to investigate this merger process that produces the most vigorous convection and the vast majority of rainfall (Keenan et al. 1994).

The vertical section of Z_{HH} in Fig. 9b shows T1 is the dominant complex with echo tops to 18 km, 26–38 dBZ echoes extending to 15-km height, and Z_{HH} values greater than 50 dBZ near 4-km height. Cells from T2 are generally less than 10 km high. A cirrus anvil is also evident from 10 to 12-km height in the region of T2. The cells within M were growing rapidly at the time shown extending to 14-km height. Peak Z_{HH} values within the cells of M were greater than 30 dBZ and were deeper to the east. The deep cell near $x = 14$ had 30-dBZ reflectivities from 2 to 8 km in height with peak reflectivities of 40–45 dBZ near 5-km height. In the

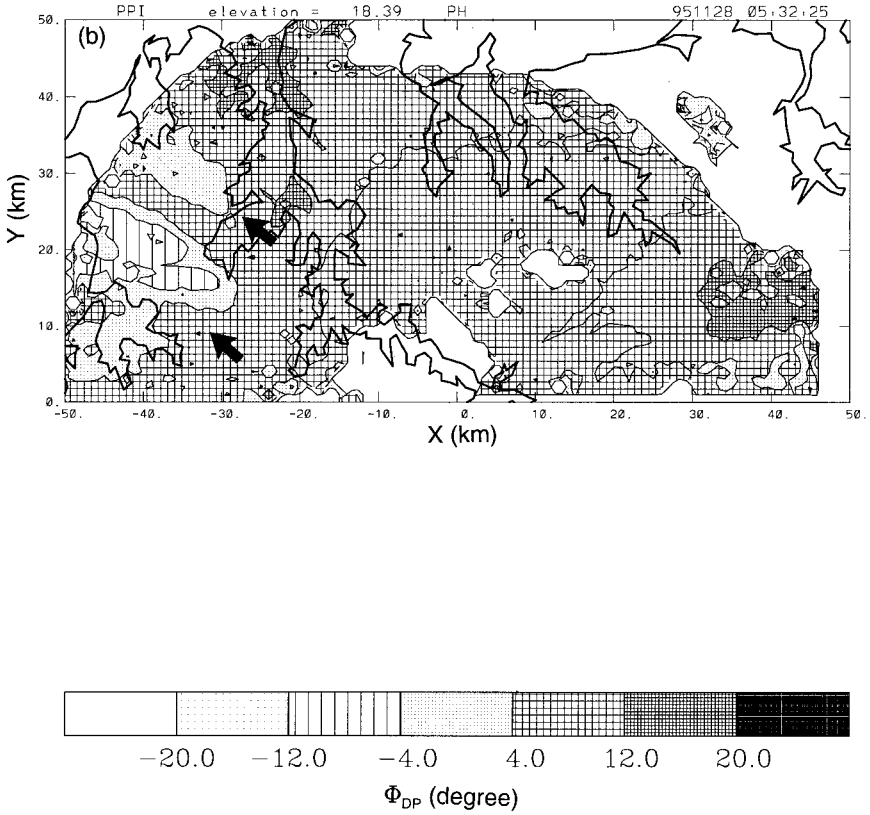

FIG. 10. (*Continued*)

region of the ''bridging'' echo ($-5 < x < 25$), the Z_{DR} values are greater than 1 dB*Z* from 2- to 7.5-km height. Maximum Z_{DR} values of greater than 3.5 dB*Z* occur near $x = 20$ km from 2.5- to 5-km height. The implication is that with $Z_{HH} > 30$ dB*Z* and $Z_{DR} > 1$ dB*Z* and the gradual increase in the height of reflectivity maximum in the more mature cells, copious supercooled rainwater existed in the bridging zone. The availability of this supercooled water could well provide an additional source of energy through release of latent heat of fusion—that is, the C-POL data indicates a possible microphysical feedback on the storm dynamics.

Within the main complex T1, there is an extensive area of negative Z_{DR} values from 2- to 7-km height for $35 < x < 45$. This region is thought to be affected by differential attenuation. Other negative Z_{DR} values are evident in low signal noise ratio situations and in regions of high reflectivity gradients. Mismatches in antenna patterns for the two polarizations (Herzegh and Carbone 1984) may well be responsible for the production of these negative Z_{DR} values. Note that the data presented here has not been edited to eliminate such spurious effects.

c. Anvil properties

The Z_{HH} and Φ_{DP} values observed within the top/anvil region (~10-km height) of an MCTEX thunderstorm are shown in Fig. 10. Throughout most of the anvil Φ_{DP} is steadily increasing radially away from the radar as expected. However, on the western edge of the complex near (−30, 15) a region of decreasing Φ_{DP} is evident. The Z_{HH} values range from 20 to 35 dB*Z* in the region and Z_{DR} values (not shown) are typically between −0.5 and 0.5 dB*Z*. These observations suggest ice particles that are being oriented vertically. The reason for this is not clear, although development of intense electric fields may be a cause, as suggested by Metcalf (1995).

6. Summary

The development of C-POL, the first Australian meteorological polarimetric radar system, has been described. The system was developed in an evolutionary manner using an existing BOM operational C-band radar as the basis. C-POL transmits linear horizontal and vertical polarizations on a pulse-to-pulse basis providing simultaneous Doppler and standard polarimetric parameters employing the algorithm of Zahrai and Zrnić (1993). The radar employs a center-feed parabolic dish without a radome with the pedestal and antenna mounted on two sea containers. The whole system is portable and can be operated in remote locations, requiring minimum infrastructure to support its installation.

Initial data collected during deployment of the radar

for MCTEX suggests that C-POL is functionally capable of supporting operations required in research programs and providing research-quality data. The operation at C band does makes it susceptible to attenuation and Mie scattering effects even in rain. However, useful data have been collected, indicating considerable potential for attenuation correction, rainfall estimation, and characterization of the vertical profile of hydrometeors.

Work is now under way to evaluate the potential of the C-POL polarimetric variables to provide quantitative rainfall measurements.

Acknowledgments. Many people contributed to the success of this project and in particular thanks are extended to Alf West (BOM), Mike Manton (BOM), Rit Carbone (NCAR), Jim Wilson (NCAR), Brian Lewis (NCAR), Peter Hildebrand (NCAR), and Douglas Hayman (CSIRO). NCAR is sponsored by the U.S. National Science Foundation.

REFERENCES

Aydin, K., and V. Giridhar, 1992: C-band dual-polarization radar observables in rain. *J. Atmos. Oceanic Technol.,* **9,** 383–390.

——, T. A. Seliga, and V. Balaji, 1986: Remote sensing of hail with a dual linear polarization radar. *J. Appl. Meteor.,* **25,** 1475–1484.

——, V. N. Bringi, and L. Liu, 1995: Rain-rate estimation in the presence of hail using S-band specific differential phase and other radar parameters. *J. Appl. Meteor.,* **34,** 404–410.

Bringi, V. N., and A. Hendry, 1990: Technology of polarization diversity radars for meteorology. *Radar in Meteolorology,* D. Atlas, Ed., Amer. Meteor. Soc., 153–190.

——, V. Chandrasekar, N. Balakrishnan, and D. S. Zrnić, 1990: An examination of propagation effects in rainfall on radar measurements at microwave frequencies. *J. Atmos. Oceanic Technol.,* **7,** 829–840.

Cary, R. H. J., 1986: The handbook of antenna design. *Radomes,* 2d ed., A. W. Rudge, K. Milne, A. D. Olver, and P. Knight, Eds., Vols. 1 and 2, Peter Peregrinus, 1151–1246.

Chandrasekar, V., and R. J. Keeler, 1993: Antenna pattern analysis and measurements for multiparameter radars. *J. Atmos. Oceanic Technol.,* **10,** 674–683.

——, V. N. Bringi, G. R. Gray, and R. J. Keeler, 1989: Efficient differential refelectivity processing using logarithmic receivers. *J. Atmos. Oceanic Technol.,* **6,** 663–670.

Collier, C. G., 1995: *COST 75 Weather Radar Systems.* European Commission, 815 pp.

Doviak, R. J., and D. S. Zrnić, 1993: *Doppler Radar and Weather Observations.* Academic Press, 562 pp.

Frush, C. L., 1984: Using the sun as a calibration aid in multiple parameter meteorological radars. *Proc. 22d Conf. on Radar Meteorology,* Zurich, Switzerland, Amer. Meteor. Soc., 306–311.

Green, A. W., 1975: An approximation for the shapes of large rain drops. *J. Appl. Meteor.,* **14,** 1578–1583.

Herzegh, P. H., and R. E. Carbone, 1984: The influence of antenna illumination function characteristics on differential reflectivity measurements. Preprints, *22d Conf. on Radar Meteorology,* Zurich, Switzerland, Amer. Meteor. Soc., 281–286.

Holt, A. R., 1995: Extracting weather forecast information from polarisation and Doppler radar data. *COST 75 Weather Radar Systems,* C. G. Collier, Ed., European Commission, 492–497.

Keenan, T., and Coauthors, 1994: Science plan—Maritime Continent Thunderstorm Experiment. BMRC Research Rep. 44, 61 pp. [Available from Bureau of Meteorology Research Centre, GPO Box 1289K, Melbourne, Victoria 3001, Australia.]

Lutz, J., P. Johnson, B. Lewis, E. Loew, M. Randall, and J. VanAndel, 1995: NCAR's SPOL portable polarimetric C-band radar. Preprints, *Ninth Symp. on Meteorological Observations and Instrumentation,* Charlotte, NC, Amer. Meteor. Soc., 408–410.

Marshall, J. S., and W. Palmer, 1948: The distribution of raindrop width size. *J. Meteor.,* **5,** 165–166.

Metcalf, J. I., 1990: Technology of polarization diversity radars for meteorological use: Panel report. *Radar in Meteorology,* D. Atlas, Ed., Amer. Meteor. Soc., 323–347.

——, 1995: Radar observations of changing orientations of hydrometeors in thunderstorms. *J. Appl. Meteor.,* **34,** 757–772.

Mueller, E. A., S. A. Rutledge, V. N. Bringi, D. Brunkow, P. C. Kennedy, K. Pattison, R. Bowie, and V. Chandrasekar, 1995: CSU-CHILL upgrades. Preprints, *27th Conf. on Radar Meteorology,* Vail, CO, Amer. Meteor. Soc., 703–706.

Ryzhkov, A. V., and D. S. Zrnić, 1995: Precipitation and attenuation measurements at a 10-cm wavelength. *J. Appl. Meteor.,* **34,** 2121–2134.

Sachidananda, M., and D. Zrnić, 1987: Rain rate estimates from differential polarization measurements. *J. Atmos. Oceanic Technol.,* **4,** 588–598.

Simpson, J., R. F. Adler, and G. R. North, 1988: A proposed Tropical Rainfall Measuring Mission (TRMM) satellite. *Bull. Amer. Meteor. Soc.,* **69,** 278–295.

Steiner, M., R. A. Houze Jr., and S. E. Yuter, 1995: Climatological characterization of three-dimensional storm structure from operational radar and rain gauge data. *J. Appl. Meteor.,* **34,** 1978–2007.

Ussailas, J. S., and J. I. Metcalf, 1983: Analysis of a polarization diversity meteorological radar design. Preprints, *21st Conf. on Radar Meteorology,* Edmonton, AB, Canada, Amer. Meteor. Soc., 331–338.

Xiao, R., V. N. Bringi, D. Garrick, E. A. Mueller, and S. A. Rutledge, 1993: Copolar and crosspolar pattern measurement of the CSU-CHILL antenna. Preprints, *26th Int. Conf. on Radar Meteorology,* Norman, OK, Amer. Meteor. Soc., 363–365.

Zahrai, A., and D. S. Zrnić, 1993: The 10-cm-wavelength polarimetric weather radar at NOAA's National Severe Storms Laboratory. *J. Atmos. Oceanic Technol,* **10,** 649–662.

Zrnić, D. S., 1996: Weather radar polarimetry—Trends toward operational applications. *Bull. Amer. Meteor. Soc.,* **77,** 1529–1534.